High Throughput Photonic Time Stretch Optical Coherence Tomography with Data Compression

C. K. Mididoddi, F. Bai, G. Wang, J. Liu, S. Gibson, and C. Wang, *Member, IEEE*

(Invited Paper)

***Abstract*—Photonic time stretch enables real time high throughput optical coherence tomography (OCT), but with massive data volume being a real challenge. In this paper, data compression in high throughput optical time stretch OCT has been explored and experimentally demonstrated. This is made possible by exploiting spectral sparsity of encoded optical pulse spectrum using compressive sensing (CS) approach. Both randomization and integration have been implemented in the optical domain avoiding an electronic bottleneck. A data compression ratio of 66% has been achieved in high throughput OCT measurements with 1.51 MHz axial scan rate using greatly reduced data sampling rate of 50 MS/s. Potential to improve compression ratio has been exploited. In addition, using a dual pulse integration method, capability of improving frequency measurement resolution in the proposed system has been demonstrated. A number of optimization algorithms for the reconstruction of the frequency-domain OCT signals have been compared in terms of reconstruction accuracy and efficiency. Our results show that the L1 Magic implementation of the primal-dual interior point method offers the best compromise between accuracy and reconstruction time of the time-stretch OCT signal tested.**

***Index Terms*—Optical coherence tomography, dispersion, photonic time stretch, compressive sensing.**

I. Introduction

OPTICAL coherence tomography (OCT) is an indispensable tool for high-resolution cross-sectional optical imaging of the internal structure of an object. Since its invention [1], OCT has been used and further improved as an in-vivo diagnostic tool for biological materials such as ocular structures [2]. On the other hand, since OCT provides high-resolution depth-resolved images of strongly scattering media in a contact-free way, this technique has also been proposed for non-biological applications, such as non-destructive testing (NDT) and contactless material characterization [3]. High-speed OCT is highly desirable for NDT applications where fast image acquisition is essential. Examples include observation of rapid dynamic processes and inspection of fast moving objects without motion artifacts.

The discovery of frequency-domain OCT has provided higher scan rate, offering greater stability and better signal-to-noise ratio compared to traditional time domain OCT methods [4]. In the last decade, extensive efforts have been made to increase the utility of frequency-domain OCT towards further higher measurement speed. Impressive MHz axial scan rates have been achieved by using a new type of high-speed frequency-sweeping optical source based on Fourier-domain mode locking (MDFL) [5], and by using channelized optical spectrum measurement with photodiode arrays [6]. Apart from targeting high-speed axial scanning, master–slave interferometry [7] was recent reported as an alternative high-speed solution for real-time en-face display of frequency-domain OCT images.

Most recently, the photonic time-stretch (PTS) technique [8], [9], also known as dispersive Fourier transform [10]-[12], real-time Fourier transform [13], [14], or wavelength-to-time mapping [15]-[17], has also been explored in high-speed OCT to provide even higher axial scan rates [18]-[21]. This method uses large chromatic dispersion in optical fibres to map the broadband spectrum of an ultrashort optical pulse into a temporal waveform. Therefore, frequency-domain OCT measurement can be achieved alternatively in time-domain using a high-speed single-pixel photodetector (PD), which enables PTS-OCT to operate at the axial scan rate equivalent to the pulse repetition rate of the laser, typically ranging from tens of MHz to even GHz. PTS-OCT was first implemented in the fiber-optic communication band (i.e., ~1550 nm) [18], in which ultrafast PDs and good dispersive elements with large dispersion-to-loss ratio are commercially available. PTS-OCT operating at a shorter wavelength range has also been implemented offering better axial resolution and less water absorption in biological samples [19]. Amplified time stretch OCT with greatly improved sensitivity based on broadband Raman amplification has been recently demonstrated to allow high-speed OCT imaging of biological tissues [20], [21].

While the PTS technique has enabled high-throughput OCT measurement thanks to the use of high-speed hardware borrowed from optical communication systems, the instruments inherently produce an extremely high-rate data

Manuscript received March 31 2017. This work was primarily supported by the Royal Society under grant RG150036, in part by the EU H2020 RAPID Project under grant 643297 and in part by Innovate UK under grant 131989. The work of C. W. was supported in part by the EU FP7 Marie-Curie Career Integration Grant under grant 631883.

C. K. Mididoddi, G. Wang and C. Wang are with the School of Engineering and Digital Arts, University of Kent, Canterbury CT2 7NT, U.K. (e-mail: c.wang@kent.ac.uk).

F. Bai and S. Gibson are with the School of Physical Sciences, University of Kent, Canterbury, CT2 7NH, U.K.

J. Liu is with VisionMetric Ltd, Canterbury, CT2 7FG, U.K.

stream. For example, for a PTS-OCT system running at an axial scan rate of nearly 100 MHz [19], with each OCT waveform having one thousand sampled pixels, and a high-speed analog-to-digital convertor (ADC) with a typical 10 bits of digitization accuracy [13], the produced data rate can be as high as one trillion bits per second. This deluge of OCT image data will overwhelm even the most advanced data acquisition circuits and the backend digital signal processors. Most electronic solutions fall short in this case due to the electronic bottleneck in speed and bandwidth. Therefore, new and efficient photonic approaches, which feature ultrafast speed and extremely broadband bandwidth, are highly demanded to address the emerging massive data problems in ultrafast OCT systems.

Compressive sensing (CS) has been recently proved as a promising data compression method [22], [23]. The CS approach is based on the fact that most natural images/signals are sparse in the wavelet domain and can be reconstructed from down-sampled data or a reduced number of measurements in a single-pixel receiver scheme such as the PTS-OCT system presented in this paper, leading to overall compressed data volume. Since the introduction of CS theory, a number of photonic CS systems have been implemented in the optical domain thanks to the huge instantaneous bandwidth of optical systems for random mixing [24] and integration [25]. Photonics-assisted CS has been successfully implemented to achieve data compression in broadband radio frequency (RF) signal detection [26]-[30], photonic time stretch ADC [24], [31]-[36], and ultrafast photonic time stretch imaging [37]-[40].

Research efforts have also been made to explore the use of CS method in OCT systems for data compression. For example, in [41], a CS method has been employed in post processing to reconstruct 3D OCT images from a subset of the original images by exploiting the image sparsity in certain transform domain. In [42], CS has been implemented in spectral domain OCT to reduce the total amount of original data from a CCD camera. The random under-sampling of OCT spectral data was achieved by randomly addressing the pixels in the CCD camera or applying a pre-set k-space mask [43]. Various reconstruction algorithms based on non-local approach [44] and energy-guided learning approach [45] have been studied to produce better reconstruction results from under-sampled data sets. Graphics processing units (GPU)-based parallel processing has improved reconstruction speed and achieved real-time CS spectral domain OCT [46].

Despite extensive studies on applying CS approach in spectral domain OCT [42]-[46], surprisingly, very little research work on data-compressed PTS-OCT has been reported so far [47], especially considering the fact that PTS-OCT suffers much more from massive data issues due to its high-throughput nature. In this work, photonic CS enabled data compression in high throughput PTS-OCT has been explored and experimentally demonstrated. Both random mixing and signal integration are implemented in the optical domain based on temporal modulation of time stretched optical pulse using pseudorandom binary sequences (PRBSs) and pulse compression using opposite dispersion value. The proposed method not only overcomes the bottleneck of big data problems [48] but also provides an economic alternative to high-speed PTS-OCT data acquisition as a very low speed (50MHz) detector is capable enough to capture compressed OCT data, which otherwise demands tens of GS/s sampling rate [18]-[21].

Some preliminary experimental observations have been recently reported by us [49]. To provide a better understanding of the proposed approach, a comprehensive analysis and further simulation and experimental verifications are presented in this paper. A data compression ratio of 66% has been achieved in high throughput OCT measurements with 1.51 MHz axial scan rate using greatly reduced data sampling rate of 50 MS/s. Furthermore, a dual pulse integration method has been demonstrated to show the capability of improving frequency measurement resolution in the proposed system. A number of optimization algorithms for the reconstruction of the frequency-domain OCT signals have also been compared in terms of frequency reconstruction accuracy and efficiency. Suggestions have been given on selection of reconstruction algorithm in CS PTS-OCT systems.

The remainder of this paper is organized as follows. In Section 2, we first describe the principle of the proposed CS PTS-OCT system in details. Section 3 presents the simulation results to verify the optical system for randomization and integration with reconstruction algorithm. Experimental demonstration of data compressed PTS-OCT for a single-layer sample with various depth profiles is carried out and presented in Section 4. A new optical compressive sensing scheme based on dual pulse compression to improve the reconstruction frequency resolution is demonstrated and reported in Section 5. In Section 6, our evaluation of a number of reconstruction algorithms for CS PTS-OCT is presented. Discussions on potential improvement in compression ratio are provided in Section 7. Finally, we summarize and conclude our work in Sections 8.

II. Principle

Schematic diagram of our proposed CS PTS-OCT system is shown in Figure 1. The optical source is a passively mode-locked laser (MLL) that produces a series of broadband ultra-short optical pulse train. The optical pulse is first stretched by a dispersion compensating fiber (DCF) generating a broadband passive wavelength swept optical carrier. The stretched pulse is then sent to a Michelson interferometer for real-time spectral-domain OCT measurement. Each frequency component of the pulse spectrum hence illuminates the sample successively in time. The back-reflected pulses from different layers of the sample are interferometrically combined with an unmodulated pulse reflected from a reference mirror at the optical coupler, resulting in an interference fringe in the time domain. The concept of PTS-OCT can also be understood based on frequency-to-time mapping: depth information of the sample is first encoded to optical pulse spectrum, which is

further mapped to a temporal waveform by large group velocity dispersion (GVD) of the DCF. The frequency-to-time mapping relation is characterized as $\lambda = t\ddot{\Psi}^{-1}$, where $\ddot{\Psi}$ is the total chromatic dispersion (in ps/nm) of the DCF. Finally a spectral interferogram can be captured in real time using a high-speed single-pixel photodetector.

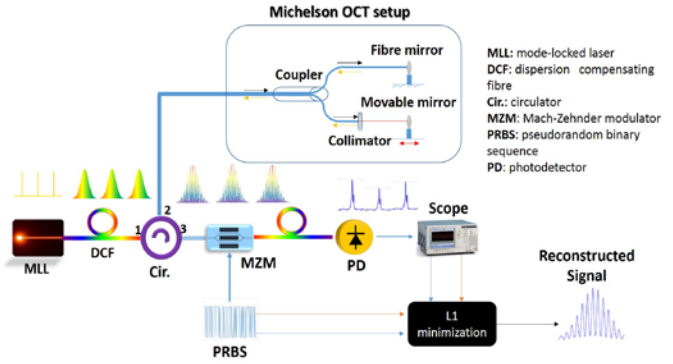

Fig. 1. Block diagram of the proposed compressive sensing PTS-OCT system.

In the Michelson-type interferometer set up, one optical fibre arm ends with a fixed fibre Faraday mirror and other arm is focused onto a moveable mirror, which emulates a single reflection-layer sample. This interferometer set up produces an interference fringe pattern in both the time and frequency domains. The optical path length difference between two arms is considered to be

$$\Delta l = \left(n_g L - L_1\right) \tag{1}$$

where n_g is the refractive index of the fibre core in the fixed arm, L is the optical fibre length in fixed arm, and L_1 is the free space distance between the fibre end and the movable reference mirror. The free spectral range (FSR) in interference spectrum in terms of optical wavelength can be calculated as

$$\Delta\lambda = \frac{\lambda^2}{2\Delta l} \tag{2}$$

Thanks to the dispersion-induced wavelength-to-time mapping, this interference spectrum is converted to a temporal interference pattern with its period given by $\Delta t = \Delta\lambda \times \ddot{\Psi}$. It can be easily deduced from Eq. (2) that the relation between RF frequency of the interference pattern and optical path length difference can be established as

$$f_{RF} = \frac{1}{\Delta t} = \frac{2\Delta l}{\lambda^2 \ddot{\Psi}} \tag{3}$$

Therefore, the optical path length difference and hence the depth information of the sample can be uniquely determined from the RF frequency at a refresh rate identical to the pulse repetition rate.

Compressive sensing theory shows that a frequency-sparse signal, such as the time-encoded OCT signal, can be recovered from a reduced number of measurements in a single-pixel receiver scheme such as the PTS-OCT system, which leads to significant data compression. Compressive sensing normally involves three successive steps [22]: random mixing, integration (or equivalently low-pass filtering), and down-sampling. The original signal can be then reconstructed following a minimization algorithm. To implement photonic compressive sensing in the optical domain, each of the spectrally encoded pulses are modulated with a pseudo-random bit sequence (PRBS) at an electro-optical modulator. The bit rate of the PRBS defines Nyquist rate of the detection system.

Assuming that the spectrally encoded and time stretched optical pulse, y is sampled at Nyquist rate with length N and sparse in Discrete Fourier Transform (DFT) domain $\Psi_{N\times N}$, the DFT domain signal can be represented as,

$$s_{N\times 1} = \Psi_{N\times N} y_{N\times 1} \tag{4}$$

The signal vector y is mixed with m PRBS patterns $\varphi_{m\times N}$, each having length N. Each randomly mixed optical pulse is integrated via optical pulse compression using a length of single mode fibre (SMF) that has opposite dispersion profile compared to DCF. This generates a down-sampled (m×1) measurement vector z, which can be represented as,

$$z_{m\times 1} = A_{m\times N} s_{N\times 1} \tag{5}$$

where $A = \varphi\Psi^{-1}$. Measurements z can be obtained by taking the optical power of each compressed pulse using a low-speed photodetector. Finally, the reconstruction of DFT domain signal from down-sampled measurements is achieved using the measurements and corresponding PRBS patterns as the inputs to an L-1 minimization program. Solving the minimization problem,

$$\min\left(\|s\|_1\right) \quad \textit{subject to} \quad z = As \tag{6}$$

results in sparse solution s, which can be used to calculate depth profile of the sample based on Eq. (3). The compression ratio is defined as m/N.

III. Simulation Results

A simulation is first performed using a commercial simulation tool VPItransmissionMaker to verify the method. The schematic shown in Fig. 1 is considered and we assume that the input optical pulse has a Gaussian shape with a full-width at half maximum (FWHM) of 800 fs and repetition rate of 50MHz, and the DCF has total dispersion of 1.28 ns/nm. The original ultrashort optical pulse is significantly stretched in time after dispersion as shown with dashed line envelop in Fig. 2a. The sample used in the simulation has a two-layer structure with a layer-to-layer separation of 0.768 mm. After reflection from the Michelson interferometer, the spectral interferogram is mapped to a time-domain waveform due to the frequency-to-time mapping. The obtained waveform is shown in Fig. 2a with solid line. Since reflection from each layer within the sample turns into unique frequency with respect to

the reference arm, each path length difference converts to a single-tone RF frequency in time domain. Figure 2b shows the corresponding Fourier transform spectrum, which has two strong frequency peaks at 4 GHz and 3.5 GHz respectively. The power of the peaks indicates the strength of reflection from individual layers. An excellent match with the given model in Eq. (3) is observed. Note that there is an additional frequency component close to the baseband, which is corresponding to inter-layer interference and can be removed during post-processing.

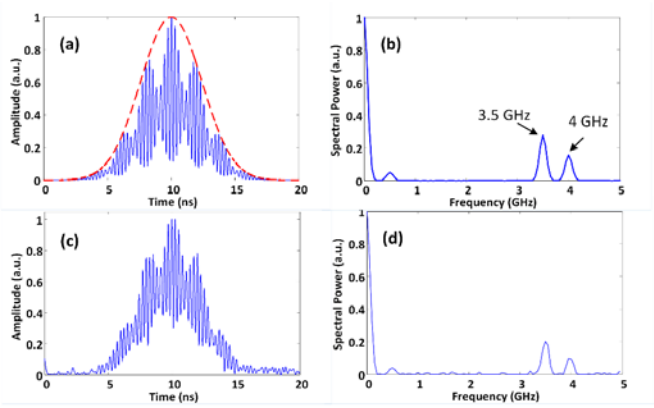

Fig. 2. Simulation results for a two-layer PTS-OCT measurement. (a) Temporal interference pattern as a result of path length difference. The time-stretched original pulse is shown in red dotted line. (b) The spectrum profile of the optical interference pattern, clearly showing two carrier frequencies of 3.5 GHz and 4 GHz. (c) The reconstructed signal in time domain using 70 measurements. (d) The reconstructed Fourier spectrum showing two strong tones which match with the original signal.

The encoded and stretched optical pulse carrying depth information is then mixed with a PRBS pattern of 10 Gbps, which leads to an original signal length of N=200. Signal integration is realized based on pulse compression using a Single mode Fibre (SMF) with opposite dispersion profile, which generates a single measurement result. Multiple measurements are implemented with different PRBS patterns and used to run L1 minimization reconstruction. By taking 70 measurements, the reconstructed DFT domain signal is shown in Fig. 2d and corresponding time domain representation is calculated using inverse Fourier transform and shown in Fig. 2c. It is evident that a good reconstruction is obtained with a compression ratio of 35%.

IV. Experimental Results

To verify the utility of the proposed compressive sensing PTS-OCT system, a proof of concept experiment has been designed and implemented based on the setup shown in Fig. 1. In the experiment, the optical source is a passively mode locked laser (Calmar Mendocino FP laser), which produces a series of ultrashort optical pulses with FWHM of 800 fs and repetition rate of 50MHz. After being time stretched using a DCF with total dispersion of 1.04ns/nm, the optical pulses are directed to a Michelson-type OCT setup where one arm is an optical fibre ended with a fibre Faraday mirror and the other is in free-space towards a moveable mirror emulating as a single-layer sample. Tuning to a particular path difference, the depth profile is encoded into the RF frequency of the mapped temporal waveform.

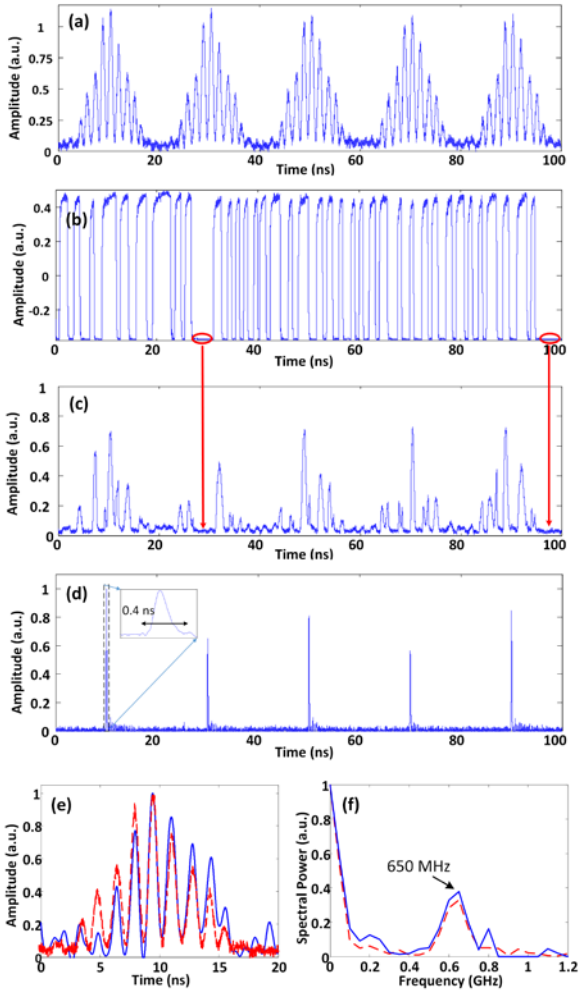

Fig. 3. Experiment results for a single-layer PTS-OCT measurement. (a) The temporal interference pattern for five successive pulses. (b) The first 5 PRBS patterns. (c) The modulated waveforms with red marking showing no pattern for exact amount of duration of a bit 0. (d) The compressed optical pulses using a SMF with opposite dispersion profile. The peak power of compressed pulses produce the measurements. (e) Overlapped temporal waveforms for the reconstructed signal (in solid line) and the original signal (in red dash line). (f) Fourier domain representation of the reconstructed signal (in solid line) and the original signal (in red dash line).

The first five consecutive pulses are captured using a high-speed PD and a real-time oscilloscope and shown in Fig. 3a. We can see the stretched Gaussian pulse is encoded with a single tone RF frequency indicating the strong single-layer reflection from the sample. The Fourier transform of the interference waveform is indicated by the red dotted line in Fig. 3e. A clear peak at 650 MHz is obtained, which corresponds to an optical path length difference of 0.81 mm. PRBS patterns at 2.5 Gbps are generated by an arbitrary waveform generator (AWG, Tektronix AWG7122C) as shown in Fig. 3b. Considering Nyquist rate of 2.5 Gbps and pulse period of 20 ns,

the original signal length is N=50. Mixing of PRBS patterns with the encoded optical pulses is implemented using a 10 GHz Mach-Zehnder modulator (MZM) with the results captured by the oscilloscope and shown in Fig. 3c. Passing the randomly mixed pulses through a SMF with opposite dispersion profile, signal integration has been realized via pulse compression. The compressed pulses are detected with a 2.5GHz PD and shown in Fig. 3d. The pulses have a pulse-width of 0.4 ns which is inversely proportional to the PD bandwidth. The peak power of each pulse indicates the integration of mixed optical pulse and leads to a single measurement result. Overall 33 measurements have been taken to reconstruct the original signal following an L1 Magic minimization algorithm as described in [50]. The reconstructed DFT domain signal is shown with solid line in Fig. 3e. We can see that the target frequency (650 MHz) has been successfully recovered with a compression ratio of 66%. Figure 3f shows the reconstructed time domain signal and the original signal with blue solid and red dotted line respectively. A good match in time-domain reconstruction has been achieved. Data compression is achieved in PTS-OCT at the cost of reduced axial scan rate. The effective axial scan rate in this experiment is 1.51 MHz. A better compression ratio (due to fewer number of measurements) will increase the scan rate as well.

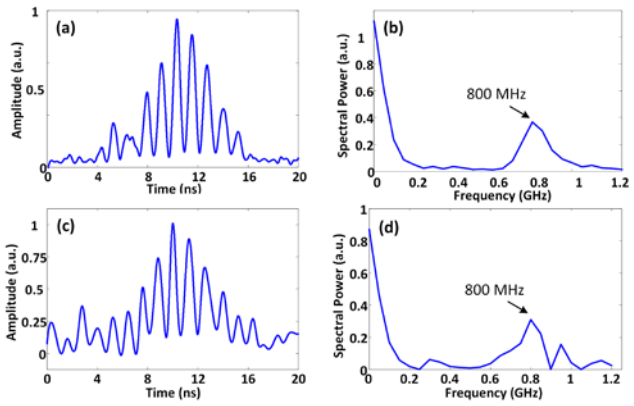

Fig. 4. Experimental results for a second single-layer sample with different path length difference. (a) The original interference pattern in time domain. (b) Fourier transform of the original interference pattern showing a single carrier frequency of 800 MHz. (c) The reconstructed time domain waveform with 33 measurements. (d) The reconstructed DFT domain signal clearly identifying the 800 MHz frequency component.

A second experiment was carried out to verify the utility of the system at different imaging depths. We tune the moveable mirror further to get an increased optical path length difference of 0.99 mm. The mapped spectrally-encoded optical pulse has a higher carrier frequency of 800 MHz, with its time-domain and frequency-domain representations shown in Figs. 4a and 4b respectively. The same random mixing and optical pulse compression processes are carried out. With 33 measurements, the reconstructed time-domain and DFT domain signals are shown in Fig. 4c and 4d respectively. The reconstructed signal matches well with the original signal with a compression ratio of 66%.

V. Improving the Frequency Detection Resolution

The compressive sensing method can efficiently reduce the total data volume as demonstrated in this paper. However, it suffers from one difficulty that it can only reconstruct discrete frequency tones (a frequency grid) in the OCT spectrum, which are harmonic tones of the laser repetition rate, due to the periodic nature of the optical pulse train. The minimum frequency resolution that can be resolved is as same as the repetition rate [51]. If the RF frequency is near a midpoint of the frequency grid, frequency detection will total fail [52]. In the application of compressive sensing PTS-OCT, this difficulty leads to only discrete depth profiles and limits its applications in practical scenarios.

More sophisticated reconstruction algorithms based on joint-sparsity-based matching pursuit has been proposed to address this issue [34]. Here we demonstrate a new optical scheme based on dual pulse integration that enables the reconstruction of non-harmonic tones using only the basic minimization algorithm. This will allow frequency reconstruction resolution less than the pulse repetition rate and unblock the detection of midpoint frequencies.

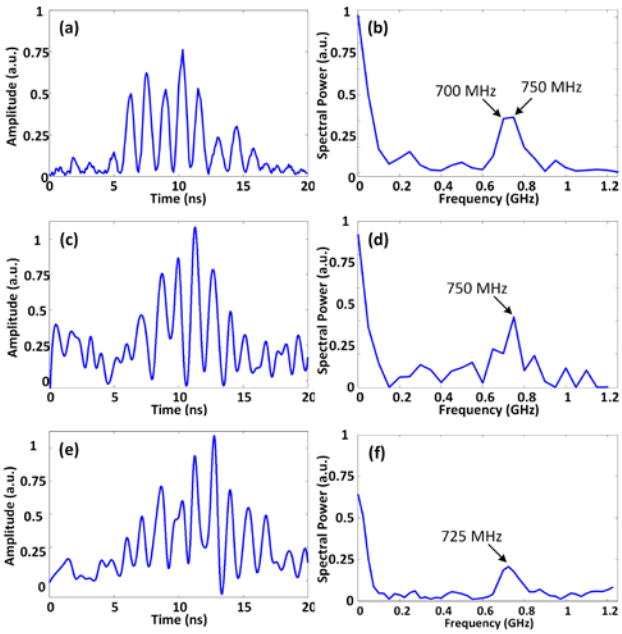

Fig. 5. Experimental results showing data compressed PTS-OCT with improved frequency resolution. (a) The original temporal interference waveform with a carrier frequency of 725 MHz. (b) Its Fourier transform shows two closely located frequency peaks at 700 and 750 MHz. (c) The constructed temporal waveform based on normal one pulse integration. (d) Reconstructed DFT signal showing only the 750 MHz signal. This indicates a total failure in frequency identification. (e) and (f) show the reconstruction results based on dual pulse integration. The 725 MHz frequency component is successfully identified.

In the experiment, the optical path length difference is set to be 0.905 mm such that the carrier RF frequency of temporal interference pattern is 725 MHz, which is obviously not a

harmonic tone of 50 MHz but a midpoint in the frequency grid with 50 MHz separation. The original spectrally-encoded temporal waveform is captured using the oscilloscope and shown in Fig. 5a and its Fourier transform is plotted in Fig. 5b. We can see that two closely located frequency peaks at 700 MHz and 750 MHz are presented due to the frequency grid. After normal compressive sensing process, the reconstructed time-domain and DFT-domain signals are shown in Figs. 5c and 5d respectively. The reconstructed frequency shows 750 MHz only and identification of actual 725 MHz frequency has totally failed. This is because 750 MHz component has a slightly higher power than 700 MHz as shown in Fig. 5b and the reconstruction algorithm only can pick up one stronger frequency. Here we integrate two successive PRBS-mixed optical pulses to form one measurement element for compressive sensing. As shown in Fig. 5f, the actual carrier frequency of 725 MHz is accurately identified thanks to dual pulse integration, and a compression ratio of 66% is achieved. Note that the detection speed has to be reduced as a trade-off.

VI. Evaluation of Minimization Algorithms in Compressive Sensing PTS-OCT

Thus far in this paper, a primal-dual interior point method for L1 minimization has been used for PTS-OCT signal reconstruction. In this section, a number of alternative optimization algorithms for the reconstruction of PTS-OCT signals have been compared in terms of their reconstruction accuracy and efficiency. This will provide useful information in selection of appropriate algorithms for this particular PTS-OCT scheme.

In the context of compressive sensing, the time-stretched measurements can be modelled as a basis pursuit or a lasso L1 minimization problem. Note that these minimization problems have a slightly different mathematical form to Eq. (6). Five sparsity promoting algorithms were compared: primal-dual interior point method (L1 Magic) [50], alternating direction method for multipliers for basis pursuit (ADMM BP) and lasso (ADMM Lasso) [54], lasso method using coordinate descent (Matlab Lasso) and its standardised version [55], and Nesterov's algorithm method (NESTA) [56].

6.1. Reconstruction accuracy

To make a fair comparison, without loss of generality, the original PTS-OCT signal is set to have four dominant carrier frequencies (2.6 GHz, 2.9 GHz, 3.6 GHz and 4.6 GHz) corresponding to a four-layer sample. A PRBS vector with probability of 0.5 and sampling rate of 10 Gbps is used to mix with the original PTS-OCT signal, which makes the overall signal length to be 200. We first show the reconstructed frequency spectrum, at a common compression ratio of 40% (80 measurements), for each of the five algorithms as shown in Fig. 6. The red line is the ground truth signal and blue line represents the reconstructed results. NESTA produces an acceptable result in which the dominant peaks are all reconstructed and L1 Magic performs similarly well. ADMM Basis pursuit produces a less noisy signal but the energy at the frequency bands of interest is suppressed, which results in a less accurate result. This is also the case for ADMM lasso. Matlab lasso produces a large frequency drift for the weakest frequency peak at 4.6 GHz.

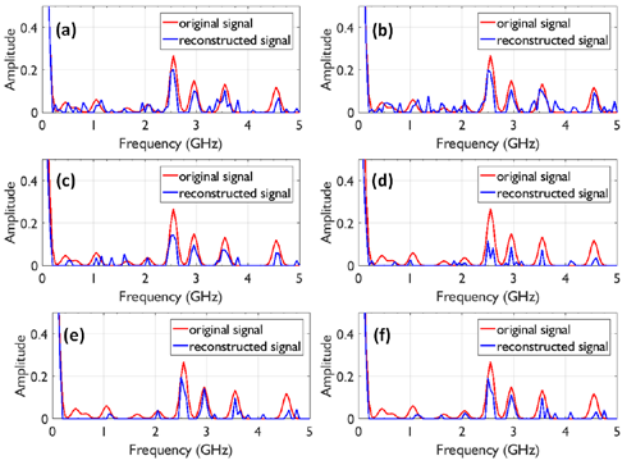

Fig. 6. The reconstructed frequency domain signals for all five algorithms corresponding to a compression ratio of 40%. Red line is the ground truth signal and blue line represents reconstruction. From left to right, top row: (a) NESTA and (b) L1 Magic; middle row: (c) ADMM Basis pursuit and (d) lasso; bottom row: (e) Matlab lasso for non-standardised data and (f) standardised data respectively.

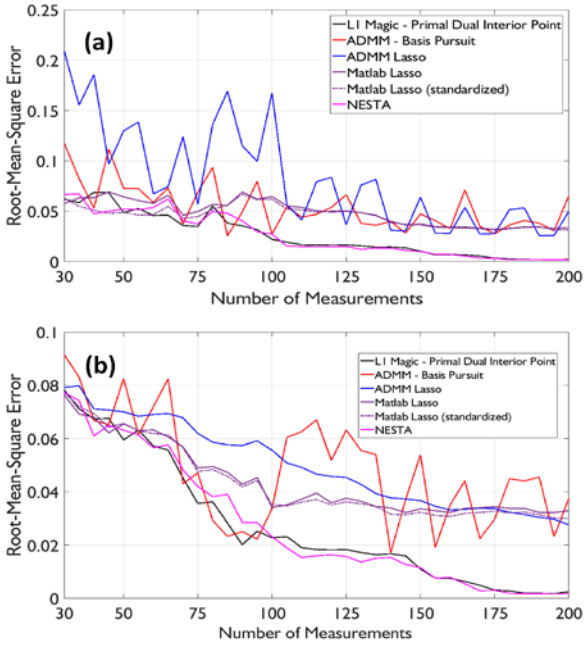

Fig. 7. Evaluation of reconstruction accuracy. (a) RMSE of reconstructed signal calculated over entire frequency range. All five candidate algorithms show a descending trend. NESTA and L1 Magic algorithm yield the smallest RMS error. (b) RMSE of reconstructed signal calculated for the frequencies spanned by the 4 dominant peaks only. Error rates similar for all five algorithms for small number of measurements. Relative performance of NESTA and L1 Magic improves as the number of measurements increases.

The reconstruction accuracy was evaluated using the root mean square error (RMSE) in the frequency domain. Reconstruction errors were first calculated, over the whole

frequency range, for different numbers of measurements ranging from 30 (15% compression ratio) up to a maximum of 200 measurements (no compression) as shown in Fig. 7a. The RMSE for the two ADMM methods is unstable but exhibits a decreasing trend w.r.t. measurements. Conversely, L1 Magic and NESTA show a smoothly decreasing error w.r.t. measurements and have the lowest error of the 5 algorithms tested. For the Matlab lasso algorithm, standardization reduces the error for fewer measurements but the error converges with non-standardised result as the number of measurements increases.

Since the four dominant frequency bands indicate the most important information, RMSE was calculated again for four dominant frequency peaks only with the results shown in Fig. 7b. Similar to Fig. 8a, NESTA and L1 Magic yield the smallest error over the frequency range. The reconstruction error for ADMM basis pursuit is again very unstable w.r.t. the number of measurements. Note at 70 to 90 measurements, ADMM basis pursuit achieves similar results to NESTA. This implies its advantage in reducing noise. In contrast, ADMM lasso remains stable at high sampling densities. Furthermore, standardisation for Matlab lasso has little effect on RMSE.

6.2. Computation cost

For each algorithm, the processing time for reconstruction was measured 5 times and averaged. The code was run in Matlab on a 64-bit Windows 10 machine with an Intel Core i7 CPU @ 3.07GHz and 8GB RAM. As shown in Fig. 8 the processing time for most algorithms is within 1 second except ADMM Basis pursuit which takes longer time than 1.5 seconds, with the peak at 2.4 seconds. This is due to its slow converge speed. ADMM is an iterative algorithm that executes quicker when the number of iterations is reduced at the expense of accuracy. The ADMM lasso is the fastest of the 5 algorithms with relatively small increase in computation time w.r.t. the number of measurements. Note, NESTA takes much more time than L1 Magic although they have similar RMSE.

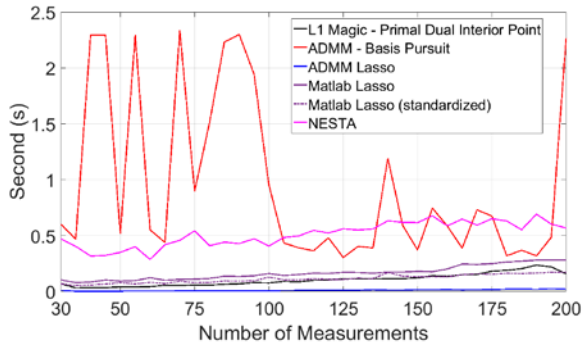

Fig. 8. The computational time as a function of the number of measurements. ADMM Lasso, Matlab Lasso, Matlab Lasso (standardized) and L1 Magic show small linear increase with respect to number of measurements. Basis pursuit is unstable for measurements < 110 due to slow convergence rate.

6.3. Summary remarks

To summarise, the five algorithms vary in performance in terms of accuracy and efficiency. For the PTS-OCT signal tested in this work, NESTA and l1 Magic algorithms produce the most reliable reconstruction accuracy. Because NESTA requires more computational time, L1 Magic can be a better choice if fast processing is important. In addition, the sparsity of original signal can affect the best compression ratio for acceptable reconstruction. According to our evaluation, the L1 Magic implementation of the primal-dual interior point method offers the best compromise between accuracy and reconstruction time of the time-stretch OCT signal tested.

VII. Discussions

In our proof-of-the-concept experimental demonstrations presented thus far, 33 measurements were required to reconstruct the original signal with a signal length of 50, leading to a compression ratio of 66%. There is great potential to improve the compression ratio based on the following three principles.

Despite a single carrier RF frequency to be identified for a single-layer sample, the reconstructed DFT domain signal is not a single-tone but a “fat” Gaussian distribution with a 3-dB bandwidth of 200 MHz. In signal reconstruction, more calculation resources and hence more measurements are required to reconstruct the whole Gaussian frequency band, which however does not carry any useful information (apart from the central peak frequency) leading to a sacrificed compression ratio. This issue can be improved by stretching the optical pulse further to a longer time window. Then the Fourier domain bandwidth will be effectively reduced. With a full-stretch of 100% duty cycle, the Fourier domain bandwidth for each carrier frequency can be as low as the pulse repetition rate [53], which is 50 MHz in our case. The compression ratio can be improved by 4 times.

Secondly, the compression ratio can be significantly improved by increasing the PRBS rate. In our demonstration, PRBS patterns are sampled at 2.5 Gbps, which is purely limited by the bandwidth of our AWG equipment. Low Nyquist rate not only limits the compression ratio but also the detection bandwidth of the PTS-OCT system. High data rate PRBS generator is a real challenge due to the electronic bottleneck. One solution is to partially compress over-stretched and PRBS-modulated optical pulse to increase the effective PRBS sampling rate [34].

Thirdly, the problem of Gaussian frequency band in the reconstructed DFT domain signal can be tackled from a different perspective. Here we use PRBS-modulated Gaussian pulse as an analog random bit sequence, rather than binary PRBS patterns as used in traditional compressive sensing systems. The use of Gaussian-shape analog random bit sequence in the reconstruction algorithm will effectively remove the Gaussian envelope of the information-carrying optical pulse and hence reduce the bandwidth of carrier frequencies in DFT domain. This method can be implemented

purely in the digital domain during signal reconstruction and no hardware changes, such as pulse over-stretching and partially compression, are required. More simulations are carried out to verify this approach with parameters as same as used in Section 3. As shown in Fig. 9, the bandwidth of frequencies of interest (3.5 and 4 GHz) has been greatly reduced due to the removal of Gaussian envelope (see inset of Fig. 9). Only 20 measurements are required to reconstruct the signal shown in Fig. 9, leading to a greatly improved compression ratio of 10%.

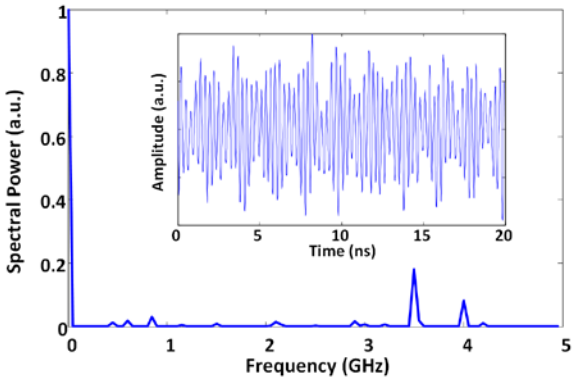

Fig. 9. Improvement of compression ratio using a Gaussian-shaped analog random bit sequence. The bandwidth of frequency peaks have been reduced. The inset shows the reconstructed temporal waveform, clearly indicating the removal of Gaussian envelope.

VIII. Summary and Conclusion

Massive data volume is an emerging challenge in high-throughput measurement systems, such as PTS-OCT. In this paper, we have proposed and experimentally demonstrated a data compression approach based on photonic compressive sensing for data-efficient time-stretch OCT systems. Random mixing and integration processes were implemented in the optical domain directly free from the electronic bottleneck. High-throughput axial scanning at 1.51 MHz has been achieved using low-speed data acquisition at 50 MS/s thanks to photonic compressive sensing with a compression ratio of 66 %. A new dual pulse integration approach has been proposed and demonstrated to improve the frequency resolution of the system. Options to further improve data compression have been exploited. A Gaussian-shape analog random bit sequence was used in the reconstruction algorithm, which leads to an improved compression ratio of 10%. In addition, a number of optimization algorithms for the reconstruction of the PTS-OCT signals have been compared in terms of reconstruction accuracy and efficiency. Our results suggest that the L1 Magic implementation of the primal-dual interior point method offers the best compromise between accuracy and reconstruction time of the time-stretch OCT signal tested.

References

[1] D. Huang, E. A. Swanson, C. P. Lin, J. S. Schuman, W. G. Stinson, W. Chang, M. R. Hee, T. Flotte, K. Gregory, C. A. Puliafito, and J. G. Fujimoto, “Optical coherence tomography,” *Science*, vol. 254, no. 5035, pp. 1178-1181, Nov. 1991.

[2] W. Drexler, U. Morgner, R. K. Ghanta, F. X. Kartner, J. S. Schuman, and J. G. Fujimoto, "Ultrahigh-resolution ophthalmic optical coherence tomography," *Nat. Med.*, vol. 7, no. 4, pp. 502-507, Apr. 2001.

[3] D. Stifter, "Beyond biomedicine: a review of alternative applications and developments for optical coherence tomography," *Appl. Phys. B: Lasers and Optics*, vol. 88, no. 3, pp. 337-357, Aug. 2007.

[4] R. Leitgeb, C. K. Hitzenberger, and A. F. Fercher, "Performance of Fourier domain vs. time domain optical coherence tomography," *Opt. Express*, vol. 11, no. 8, pp. 889-894, Apr. 2003.

[5] R. Huber, M. Wojtkowski, and J. G. Fujimoto, "Fourier Domain Mode Locking (FDML): A new laser operating regime and applications for optical coherence tomography," *Opt. Express*, vol. 14, no. 8, pp. 3225-3237, Apr. 2006.

[6] D. Choi, H. Hiro-Oka, H. Furukawa, R. Yoshimura, M. Nakanishi, K. Shimizu, and K. Ohbayashi, "Fourier domain optical coherence tomography using optical demultiplexers imaging at 60,000,000 lines/s," *Opt. Lett.*, vol. 33, no. 12, pp. 1318-1320, Jun. 2008.

[7] A. G. Podoleanu and A. Bradu, "Master–slave interferometry for parallel spectral domain interferometry sensing and versatile 3D optical coherence tomography," *Opt. Express*, vol. 21, no. 16, pp. 19324-19338, Aug. 2013.

[8] S. Gupta and B. Jalali, "Time stretch enhanced recording oscilloscope," *Appl. Phys. Lett.*, vol. 94, no. 4, pp. 041105, Jan. 2009.

[9] K. Goda, K. K. Tsia, and B. Jalali, "Serial time-encoded amplified imaging for real-time observation of fast dynamic phenomena," *Nature*, vol. 458, no. 7242, pp. 1145-1149, Apr. 2009.

[10] J. Chou, D. R. Solli, and B. Jalali, "Real-time spectroscopy with subgigahertz resolution using amplified dispersive Fourier transformation," *Appl. Phys. Lett.*, vol. 92, no. 11, p. 111102, Mar. 2008.

[11] K. Goda and B. Jalali, "Dispersive Fourier transformation for fast continuous single-shot measurements," *Nat. Photon.*, vol. 7, no. 2, pp. 102-112, Feb. 2013.

[12] C. Wang, "Dispersive Fourier transformation for versatile microwave photonics applications," *Photonics*, vol. 1, no. 4, pp. 586-612, Dec. 2014.

[13] T. Jannson, "Real-time Fourier transformation in dispersive optical fibers," *Opt. Lett.*, vol. 8, no. 4, pp. 232-234, Apr. 1983.

[14] M. A. Muriel, J. Azana, and A. Carballar, "Real-time Fourier transformer based on fiber gratings," *Opt. Lett.*, vol. 24, no. 1, pp. 1-3, Jan. 1999.

[15] C. Wang, F. Zeng, and J. P. Yao, "All-fiber ultrawideband pulse generation based on spectral-shaping and dispersion-induced frequency-to-time conversion," *IEEE Photon. Technol. Lett.*, vol. 19, no. 2-4, pp. 137-139, Feb. 2007.

[16] V. Torres-Company, D. E. Leaird, and A. M. Weiner, "Dispersion requirements in coherent frequency-to-time mapping," *Opt. Express*, vol. 19, no. 24, pp. 24718-24729, Nov. 2011.

[17] L. R. Chen, "Photonic generation of chirped microwave and millimeter wave pulses based on optical spectral shaping and wavelength-to-time mapping in silicon photonics," *Opt. Commun.*, vol. 373, pp. 70-81, 2016.

[18] S. Moon and D. Y. Kim, "Ultra-high-speed optical coherence tomography with a stretched pulse supercontinuum source," *Opt. Express*, vol. 14, no. 24, pp. 11575-11584, Nov. 2006.

[19] K. Goda, A. Fard, O. Malik, G. Fu, A. Quach, and B. Jalali, “High-throughput optical coherence tomography at 800 nm,” *Opt. Express*, vol. 20, no. 18, pp. 19 612–19 617, Aug. 2012.

[20] J. J. Xu, C. Zhang, J. B. Xu, K. K. Y. Wong, and K. K. Tsia, "Megahertz all-optical swept-source optical coherence tomography based on broadband amplified optical time-stretch," *Opt. Lett.*, vol. 39, no. 3, pp. 622-625, Feb. 2014.

[21] J. J. Xu, X. Wei, L. Yu, C. Zhang, J. B. Xu, K. K. Y. Wong, and K. K. Tsia, "High-performance multi-megahertz optical coherence tomography based on amplified optical time-stretch," *Biomed. Opt. Express*, vol. 6, no. 4, pp. 1340-1350, Apr. 2015.

[22] D. L. Donoho, "Compressed sensing," *IEEE Trans. Inf. Theory*, vol. 52, no. 4, pp. 1289-1306, Apr. 2006.

[23] J. A. Tropp, J. N. Laska, M. F. Duarte, J. K. Romberg, and R. G. Baraniuk, "Beyond Nyquist: efficient sampling of sparse bandlimited signals," *IEEE Trans. Inf. Theory*, vol. 56, no. 1, pp. 520-544, Jan. 2010.

[24] G. C. Valley, G. A. Sefler, and T. J. Shaw, "Compressive sensing of sparse radio frequency signals using optical mixing," *Opt. Lett.*, vol. 37, no. 22, pp. 4675-4677, Nov. 2012.

[25] Y. Chen, X. Yu, H. Chi, X. Jin, X. Zhang, S. Zheng, and M. Galili, "Compressive sensing in a photonic link with optical integration," *Opt. Lett*., vol. 39, no. 8, pp. 2222-2224, Apr. 2014.

[26] J. M. Nichols and F. Bucholtz, "Beating Nyquist with light: a compressively sampled photonic link," *Opt. Express*, vol. 19, no. 8, pp. 7339-7348, Apr. 2011.

[27] H. Chi, Y. Mei, Y. Chen, D. Wang, S. Zheng, X. Jin, and X. Zhang, "Microwave spectral analysis based on photonic compressive sampling with random demodulation," *Opt. Lett.*, vol. 37, no. 22, pp. 4636-4638, Nov. 2012.

[28] Y. Liang, M. Chen, H. Chen, C. Lei, P. Li, and S. Xie, "Photonic-assisted multi-channel compressive sampling based on effective time delay pattern," *Opt. Express*, vol. 21, no. 22, pp. 25700-25707, Nov. 2013.

[29] F. Yin, Y. Gao, Y. Dai, J. Zhang, K. Xu, Z. Zhang, J. Li, and J. Lin, "Multifrequency radio frequency sensing with photonics-assisted spectrum compression," *Opt. Lett*., vol. 38, no. 21, pp. 4386-4388, Nov. 2013.

[30] C. Wang and N. J. Gomes, "Photonics-enabled sub-Nyquist radio frequency sensing based on temporal channelization and compressive sensing," in *Microwave Photonics* (MWP), *2014 IEEE Topical Meeting on*, 2014, pp. 335-338.

[31] H. Chi, Y. Chen, Y. Mei, X. Jin, S. Zheng, and X. Zhang, "Microwave spectrum sensing based on photonic time stretch and compressive sampling," *Opt. Lett*., vol. 38, no. 2, pp. 136-138, Jan. 2013.

[32] B. T. Bosworth and M. A. Foster, "High-speed ultrawideband photonically enabled compressed sensing of sparse radio frequency signals," *Opt. Lett*., vol. 38, no. 22, pp. 4892-4895, Nov. 2013.

[33] Y. Chen, H. Chi, T. Jin, S. L. Zheng, X. F. Jin, and X. M. Zhang, "Sub-Nyquist sampled analog-to-digital conversion based on photonic time stretch and compressive sensing with optical random mixing," *J. Lightwave Technol*., vol. 31, no. 21, pp. 3395-3401, Nov. 2013.

[34] B. T. Bosworth, J. R. Stroud, D. N. Tran, T. D. Tran, S. Chin, and M. A. Foster, "Ultrawideband compressed sensing of arbitrary multi-tone sparse radio frequencies using spectrally encoded ultrafast laser pulses," *Opt. Lett*., vol. 40, no. 13, pp. 3045-3048, Jul. 2015.

[35] G. C. Valley, G. A. Sefler, and T. Justin Shaw, "Multimode waveguide speckle patterns for compressive sensing," *Opt. Lett*., vol. 41, no. 11, pp. 2529-2532, Jun. 2016.

[36] T. P. McKenna, J. H. Kalkavage, M. D. Sharp, and T. R. Clark, "Wideband photonic compressive sampling system," *J. Lightwave Technol*., vol. 34, no. 11, pp. 2848-2855, Jun. 2016.

[37] B. T. Bosworth, J. R. Stroud, D. N. Tran, T. D. Tran, S. Chin, and M. A. Foster, "High-speed flow microscopy using compressed sensing with ultrafast laser pulses," *Opt. Express*, vol. 23, no. 8, pp. 10521-10532, Apr. 2015.

[38] Q. Guo, H. Chen, Z. Weng, M. Chen, S. Yang, and S. Xie, "Compressive sensing based high-speed time-stretch optical microscopy for two-dimensional image acquisition," *Opt. Express*, vol. 23, no. 23, pp. 29639-29646, Nov. 2015.

[39] A. C. S. Chan, A. K. S. Lau, K. K. Y. Wong, E. Y. Lam, and K. K. Tsia, "Arbitrary two-dimensional spectrally encoded pattern generation - a new strategy for high-speed patterned illumination imaging," *Optica*, vol. 2, no. 12, pp. 1037-1044, Dec. 2015.

[40] C. Lei, Y. Wu, A. C. Sankaranarayanan, S. M. Chang, B. Guo, N. Sasaki, H. Kobayashi, C. W. Sun, Y. Ozeki, and K. Goda, "GHz optical time-stretch microscopy by compressive sensing," *IEEE Photon. J*., vol. 9, no. 2, pp. 1-8, Apr. 2017.

[41] E. Lebed, P. J. Mackenzie, M. V. Sarunic, and M. F. Beg, "Rapid volumetric OCT image acquisition using Compressive Sampling," *Opt. Express*, vol. 18, no. 20, pp. 21003-21012, Sep. 2010.

[42] X. Liu and J. U. Kang, "Compressive SD-OCT: the application of compressed sensing in spectral domain optical coherence tomography," *Opt. Express*, vol. 18, no. 21, pp. 22010-22019, Oct. 2010.

[43] N. Zhang, T. Huo, C. Wang, T. Chen, J.-g. Zheng, and P. Xue, "Compressed sensing with linear-in-wavenumber sampling in spectral-domain optical coherence tomography," *Opt. Lett*., vol. 37, no. 15, pp. 3075-3077, Aug. 2012.

[44] C. Liu, A. Wong, K. Bizheva, P. Fieguth, and H. Bie, "Homotopic, non-local sparse reconstruction of optical coherence tomography imagery," *Opt. Express*, vol. 20, no. 9, pp. 10200-10211, Apr. 2012.

[45] S. Schwartz, C. Liu, A. Wong, D. A. Clausi, P. Fieguth, and K. Bizheva, "Energy-guided learning approach to compressive FD-OCT," *Opt. Express*, vol. 21, no. 1, pp. 329-344, Jan. 2013.

[46] D. Xu, Y. Huang, and J. U. Kang, "Real-time compressive sensing spectral domain optical coherence tomography," *Opt. Lett*., vol. 39, no. 1, pp. 76-79, Jan. 2014.

[47] J. R. Stroud, B. Bosworth, D. Tran, T. D. Tran, S. Chin, and M. A. Foster, "72 MHz A-scan optical coherence tomography using continuous high-rate photonically-enabled compressed sensing (CHiRP-CS)," in *Conference on Lasers and Electro-Optics*, San Jose, California, 2016, p. SM2I.1.

[48] B. Jalali and M. H. Asghari, "The anamorphic stretch transform: Putting the squeeze on "Big Data"," *Opt. Photonics News*, vol. 25, no. 2, pp. 24–31, Feb. 2014.

[49] C. K. Mididoddi, G. Wang, and C. Wang, "Data compressed photonic time-stretch optical coherence tomography," in *IEEE Photonics Conference* (IPC), 2016, pp. 13-14.

[50] K. M. Koh, S. J. Kim, and S. Boyd, "An interior-point method for large-scale l(1)-regularized logistic regression," *J. Mach. Learn. Res*., vol. 8, pp. 1519-1555, Jul. 2007.

[51] M. Mishali and Y. C. Eldar, "From theory to practice: sub-Nyquist sampling of sparse wideband analog signals," *IEEE J. Sel. Topics Signal Process*., vol. 4, no. 2, pp. 375-391, Apr. 2010.

[52] C. V. McLaughlin, J. M. Nichols, and F. Bucholtz, "Basis mismatch in a compressively sampled photonic link," *IEEE Photon. Technol. Lett.*, vol. 25, no. 23, pp. 2297-2300, Dec. 2013.

[53] C. Wang and J. Yao, "Ultrahigh-resolution photonic-assisted microwave frequency identification based on temporal channelization," *IEEE Trans. Microw. Theory Tech.*, vol. 61, no. 12, pp. 4275-4282, Dec. 2013.

[54] S. Boyd, N. Parikh, E. Chu, B. Peleato, and J. Eckstein, "Distributed optimization and statistical learning via the alternating direction method of multipliers," *Found. Trends Mach. Learn*., vol. 3, no. 1, pp. 1-122, Jan. 2011.

[55] J. Friedman, T. Hastie, and R. Tibshirani, "Regularization Paths for Generalized Linear Models via Coordinate Descent," *J. Stat. Softw.*, vol. 33, no. 1, pp. 1-22, Aug. 2010.

[56] S. Becker, J. Bobin, and E. J. Candès, "NESTA: A fast and accurate first-order method for sparse recovery," *SIAM J. Imaging Sci*., vol. 4, no. 1, pp. 1-39, Jan. 2011.